Chapter 3

Losses in strands

The main objective of this chapter is to present a brief survey of the main loss components at strand level, namely the hysteresis loss in the filaments, the transport-current loss and the interfilament coupling loss.

The theory of the filament hysteresis and transport-current loss is discussed and general formulas are presented to describe the loss during a field change. The magnetisation due to the filament hysteresis in several LHC-type strands is experimentally determined.

The interfilament coupling loss is dealt with in detail and experimental results are given for several LHC-type strands in terms of the time constant τ_{if} which quantifies the loss. The reduction of the maximum transport current in a strand, due to the additional interfilament coupling currents is discussed. The corresponding effect of the interfilament coupling currents on the ramp-rate limitation of dipole magnets is investigated.

The influence of the magnetisation of adjacent strands on the hysteresis loss and interfilament coupling loss is experimentally investigated, by evaluating the losses within the strand for a single strand as well as for a Rutherford-type cable.

3.1 Introduction

In accelerator magnets, and especially at low excitation levels and small field-sweep rates, the energy loss and the field distortions are mainly determined by the filament hysteresis. The magnetisation or hysteresis loss is a well-understood phenomenon and it has already been shown in 1963 that the hysteresis can be reduced by the use of multifilamentary composite conductors with a small filament diameter [London, '63]. In order to provide stability and a good thermal conductivity the matrix of the conductors is generally a normal metal with a low electrical resistivity. This leads to the so-called interfilament coupling loss (IFCL) due to eddy currents in the normal matrix. The IFCL has been extensively treated by many authors and a useful publication is one by Campbell in which the IFCL and the time constant are discussed for various conductor geometries [Campbell, '82]. Detailed numerical solutions of the AC behaviour of superconducting wires have been presented during the last decade [Rem, '86], [Hartmann, '89]. Knowledge of the IFCL in the strands of a cable is necessary for separating the IFCL from the interstrand coupling loss in magnets. Only then can the origin of ramp-rate induced field-distortions and ramp-rate induced quenches in magnets be correctly evaluated.

In section 3.2 the hysteresis loss is discussed and illustrated by means of the current and field distribution over the cross-section of a filament exposed to a field cycle. It is shown that an additional transport current increases the total loss which is partially supplied by the external field and partially by the current supply.

Experimental results of the filament magnetisation are presented in section 3.3 for various cables from which the coils of the LHC dipole model magnets are wound. The analysis is made for filaments carrying no transport current exposed to field variations between -0.6 and 0.6 T at low frequency, so that the screening effect of the interfilament coupling currents (IFCCs) is small compared to the applied field. In chapter 6 the results are compared quantitatively to the hysteresis loss in entire coils.

The IFCCs are discussed in section 3.4 and it is shown that the loss can be represented by a mean time constant τ_{if}. The influence of the IFCCs, which saturate the outer layer(s) of filaments in a strand, on the maximum transport current is investigated. Experimental results are presented of τ_{if} of various cables as used in the LHC dipole model magnets and the corresponding decrease of the maximum transport current is estimated.

The influence of the neighbouring strands on the loss in a strand is discussed. This is achieved by determining not only the hysteresis loss and IFCL in a cable but also the losses in a single strand which is removed from the cable. The results and consequences for magnets are presented in section 3.5.

3.2 Hysteresis loss

If a superconducting filament without transport current is subjected to an increasing transverse magnetic field B_a, the field penetrates from the outside while the interior of the filament will remain field-free due to screening currents with density $\pm J_C$ in the outer region (see Fig. 3.1a). The contour seperating the screening currents region from the current-free region will penetrate the filament as the field increases because the critical current density is

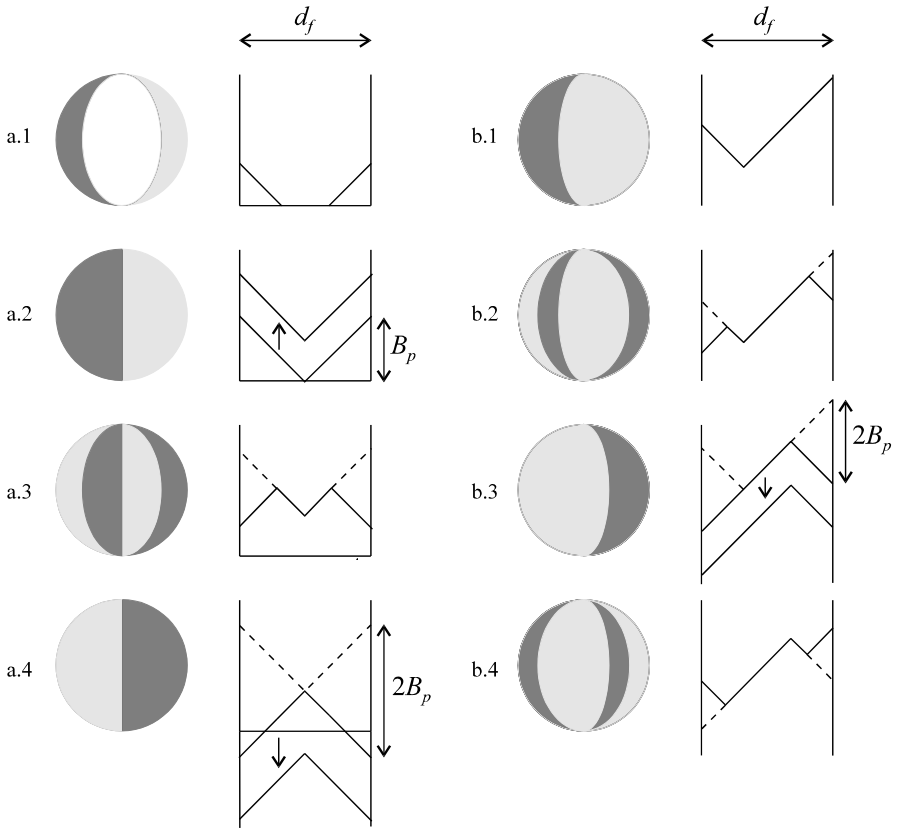

Figure 3.1. **a.** Current and field profiles of a superconducting filament without transport current in a varying external field: **1.** $B_{a,1} < B_p$, **2.** $B_{a,2} = B_p$ and larger, **3.** $B_{a,2}\text{-}2B_p < B_{a,3} < B_{a,2}$, **4.** $B_{a,4} = B_{a,2}\text{-}2B_p$ and smaller.
b. Current and field profiles of a superconducting filament carrying a transport current in a varying external field: **1.** field $B_{a,1}$, **2.** $B_{a,1}\text{-}2B_p < B_{a,2} < B_{a,1}$, **3.** $B_{a,3} = B_{a,1}\text{-}2B_p$ and smaller, **4.** $B_{a,3} < B_{a,4} < B_{a,3} + 2B_p$.

limited. The field at which the filament becomes completely penetrated is called the penetration field B_p, and is equal to:

$$B_p = \frac{\mu_0 J_C d_f}{\pi} \quad [\mathrm{T}]\,, \tag{3.1}$$

for round and isotropic filaments, with J_C the critical current density in the filament and d_f the filament diameter. The field B_p is therefore the maximum field produced by the screening currents. The magnetisation, defined as the magnetic moment per unit volume, of a fully penetrated round filament is:

$$M = -\frac{2}{3\pi} J_C d_f \,\mathrm{sgn}(\dot{B}_a) = -\frac{2}{3\mu_0} B_p \,\mathrm{sgn}(\dot{B}_a) \quad [\mathrm{Am}^{-1}]\,. \tag{3.2}$$

When the applied-field change $\dot{\mathbf{B}}_a$ reverses its sign, the filament reacts again by screening the field, so that a new contour will appear in the outer region. A further change of the applied field will change the screening current density from $+J_C$ to $-J_C$ (and the other way around), so that the field is completely penetrated after a change of $2B_p$ in the applied field (see Fig. 3.1a). A characteristic magnetisation loop is shown in Fig. 3.2 in the case of a filament with a penetration field of about 0.1 T at small fields and 0.05 T at $B_a = 0.5$ T.

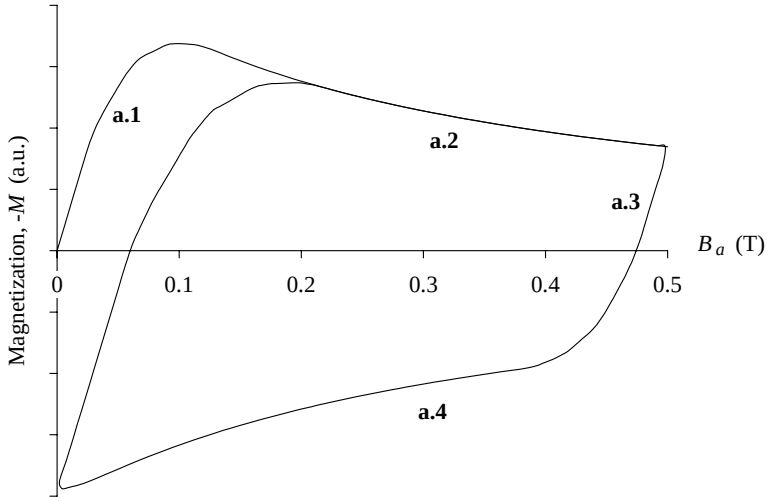

Figure 3.2. Magnetisation loop of a filament without transport current subject to a field cycle 0-0.5 T-0-0.5 T. The labels correspond to the magnetisation pattern as shown in Fig. 3.1a.

In high-field magnets, the central field is cycled between the fields B_1 and B_2 where $\Delta B = (B_2 - B_1)$ is far larger than B_p (which is of the order of 10-100 mT for multifilamentary NbTi conductors). Therefore, most of the filaments in the strands remain fully penetrated during the field sweep and the magnetisation as given by eq. 3.2 varies according to the variation of the critical current with the field. A large magnetisation at the start of the ramp leads to large relative field distortions. Because the particles have to be injected at a small field B_{inj}, the filament size has to be small in order to reduce these field errors. The field B_{inj} has to be approached coming from a smaller field so that the magnetisation of the filaments does not reverse sign at the start of the ramp. Reduction of additional field distortions, caused by coupling currents and a non-uniform current distribution among the strands (see chapter 7), impose a more complicated field cycle before and during injection.

The hysteresis loss per cycle and per unit volume is given by the area enclosed within the hysteresis loop in the *MB* plane for zero frequency:

$$Q_{hys} = -\oint M(B_a)\,dB_a \quad [\mathrm{Jm^{-3}/cycle}] \,. \tag{3.3}$$

For a field cycle between B_1 and B_2 (with $0 < B_1 < B_2 < 3$ T), the critical current density is represented by means of the Kim relation $J_C(B) = J_0 B_0 / (|B| + B_0)$ (see section 2.4) so that:

$$Q_{hys} = -2\frac{2d_f}{3\pi}\int_{B_1}^{B_2}\frac{J_0 B_0}{|B_a|+B_0}dB_a = \frac{4d_f J_0 B_0}{3\pi}\ln\left(\frac{|B_2|+B_0}{|B_1|+B_0}\right) \quad [\mathrm{Jm^{-3}/cycle}]\,. \tag{3.4}$$

The filament magnetisation for an applied field parallel to the filament is [Niessen, '93]:

$$M_{\parallel} = -\frac{1}{6}J_{C,\parallel}d_f\,\mathrm{sgn}(\dot{B}_{a,\parallel}) \quad [\mathrm{Am^{-1}}]\,, \tag{3.5}$$

but will be disregarded in this chapter since, in most applications, the angle between the applied field and the filament axis is close to 90°.

An additional transport current causes a decrease of the penetration field (see Fig. 3.1b) by a factor $(1-(I_{tr}/I_C)^2)=(1-(J_{tr}/J_C)^2)$ [Rem, '86], with J_{tr} the average current density in the filament. The magnetisation and the hysteresis loss are consequently reduced by the same factor for large field variations compared to the penetration field.

However, in the presence of a varying applied field, the transport current also causes an additional loss component which can be represented by a dynamic resistance [Druyvesteyn, '67], and results in an axial electric field over the filament [Hartmann, '89]:

$$E_{dyn} = \frac{4d_f}{3\pi}|\dot{B}_a|(J_{tr}/J_C) \quad [\mathrm{Vm^{-1}}] \quad \text{for } J_{tr} < J_C\,. \tag{3.6}$$

The additional loss component $J_{tr}E_{dyn}$ is supplied by the current source and not by the external field, and can be expressed by:

$$J_{tr}E_{dyn} = \frac{4d_f}{3\pi}J_C|\dot{B}_a|(J_{tr}/J_C)^2 \quad [\mathrm{Wm^{-3}}]\,. \tag{3.7}$$

The total energy loss Q_{hys} (i.e. the work done by the external field and the current supply) for a filament carrying a transport current and for field oscillations well above the penetration field is therefore (combining eqs. 3.2, 3.3 and 3.7):

$$\begin{aligned} Q_{hys} &= \frac{2d_f}{3\pi}\oint J_C\left(1-(J_{tr}/J_C)^2+2(J_{tr}/J_C)^2\right)dB_a \\ &= \frac{2d_f}{3\pi}\oint J_C\left(1+(J_{tr}/J_C)^2\right)dB_a \quad [\mathrm{Jm^{-3}/cycle}]\,, \end{aligned} \tag{3.8}$$

i.e. a factor $(1+(J_{tr}/J_C)^2)$ larger than the loss as given by eq. 3.3 for a filament without transport current.

In the case of a filament carrying an AC transport current and subjected to a varying external field an additional loss component is present due to the varying self-field. In a magnet where the total field is achieved through the use of small diameter wire or multistrand conductor, the self-field variation is small compared to the external-field variation arising from the rest of the turns. Hence, the self-field loss does not make a substantial contribution to the total loss and is disregarded here.

An accurate value of the hysteresis loss for field variations ΔB of the same order or smaller than B_p is calculated with a numerical model in which the cross-section of the filament is divided into discrete subregions, carrying either zero current or the critical current density. The variation in the external field and the transport current are represented by discrete steps. For each step the current in the subregions is calculated iteratively, since not only the external field but also the field generated by the other subregions determines the critical current of a subregion. A detailed description of this procedure is given elsewhere [Hartmann, '89].

The screening currents are often referred to as persistent currents as they can only be removed by driving the filament from the superconducting into the normal state. The persistent currents result in a residual field which increases with increasing filament diameter and increasing J_C (i.e. decreasing field or temperature). In accelerator magnets it is mainly this residual field that determines the acceptable filament diameter since the relative field errors can become large, especially at weak excitation. Since a high critical current density is required to have an efficient design, a decrease in the filament diameter is necessary for reducing the persistent currents.

A decrease in the filament diameter is often coupled with a decrease in the spacing b between the filaments. In the case of NbTi embedded in a copper matrix a spacing below about 1 μm results in the so called 'proximity coupling' between neighbouring filaments. This proximity coupling is basically a tunneling of the Cooper pairs through the copper matrix and results in an enhanced effective diameter of the filament at low magnetic fields. Hence, a certain optimum in the filament diameter occurs for which the persistent currents are minimum. Measurements on SSC dipole magnets have shown that for a filament diameter of about 4 μm the residual field is smallest, at a central field of 0.33 T and a ratio $b/d_f = 0.2$ [Green, '87].

3.3 The J_C-B relation

Eq. 3.2 shows that the magnetisation of a fully penetrated filament is proportional to the critical current density. The J_C-B relation of a superconductor can therefore be determined by measuring the magnetisation in an external varying magnetic field. The cold part of the test set-up by which these magnetisation measurements are performed is shown in Fig. 3.3.

It consists of a concentric set of four pick-up coils that can be inserted in a superconducting solenoid providing an AC field of 0.6 T maximum. The magnetisation is measured on a ring-shaped sample (with a circumference of 130 mm maximum) inserted between the two upper pick-up coils. This ensures that both the inductive voltage and the empty coil effect are minimum. The pick-up coils are wound from a superconducting wire and are connected to a small superconducting sensing coil. The current in the circuit is proportional to the time integral of the pick-up voltage. The circuit can be regarded as a flux transformer, where the flux change in the pick-up set, due to the magnetisation of the sample, is transferred to the sensing coil. The flux in the sensing coil is measured using a Hall probe which is placed inside a superconducting PbBi shield, in order to exclude the stray field of the solenoid and other magnetic disturbances.

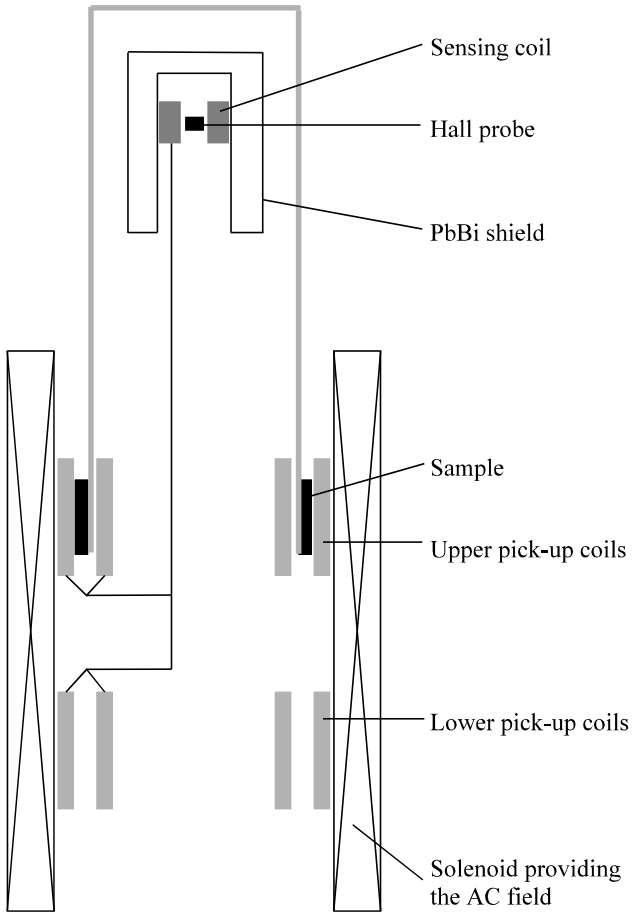

Figure 3.3. The cold part of the measuring system where the voltage of the Hall probe is a measure of the magnetisation of the sample.

Two heaters are present to enable a reset of the magnetic shield and the flux transformer in case flux has penetrated through the shield or is trapped in the flux-transformer circuit.

Characteristic measured magnetisation loops of two cables are shown in Fig. 3.4, including calculated magnetisation loops assuming the Kim relation for $J_C(B)$ (see eq. 2.16) with J_0 and B_0 as fit parameters.

Especially the cables with a small filament diameter, namely I-2 and I-4 (see Table 2.4), show a relatively large increase of the magnetisation for small fields compared to the calculated magnetisation. The enhancement is attributed to the proximity effect which can be regarded as an increase of the effective filament diameter as explained before. This results in a discrepancy between the experimental results and the calculated magnetisation since the proximity effect is not incorporated in the numerical model.

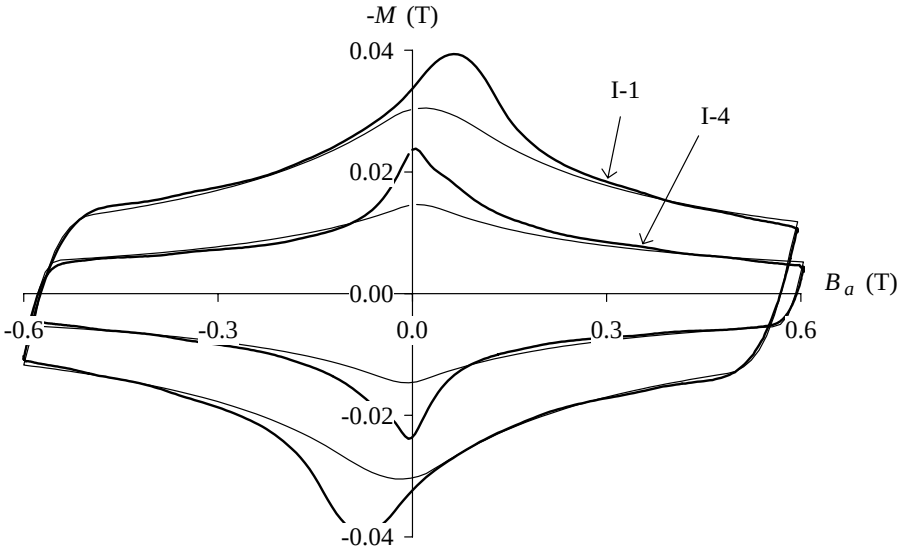

Figure 3.4. Magnetisation loops (bold lines) of cables I-1 and I-4 (see Table 2.4) subject to a sinusoidally oscillating field with an amplitude of 0.6 T and a frequency of 0.02 Hz. The thin lines are best fits, numerically calculated using the Kim relation for $J_C(B)$.

The peak in the magnetisation curve is always slightly displaced from the origin as the internal field is not zero, due to the screening currents. The displacement increases for increasing filament diameter and critical current density.

The J_C-B relation of the filament (without the matrix) is determined by fitting the numerically calculated magnetisation (using the Kim relation for $J_C(B)$ as given in eq. 2.16) to the experimentally determined magnetisation between 0.3 and 0.6 T. The results in terms of the fit parameters J_0 and B_0 are given in Table 3.1. The fit is at least valid in the field range from 0.3 to 0.6 T.

Table 3.1. Survey of the constants J_0 and B_0 of the Kim relation for several samples obtained by fitting the magnetisation loops with an amplitude of 0.6 T. The indicated critical current density at 0.6 T is the average current density over the cross-section of the strand.

	I-1	I-2	I-3	I-4	O-2
J_0 (10^{10} Am^{-2})	3.0	3.1	2.3	3.7	4.5
B_0 (T)	0.31	0.32	0.30	0.30	0.35
J_C at 0.6 T, 4.2 K (10^9 Am^{-2})	3.8	4.1	2.6	4.7	5.9

3.4 Interfilament coupling currents

The presence of a matrix results in the flow of coupling currents between the filaments of a strand when it is exposed to a changing magnetic field. Contrary to a normal conductor, specific current paths occur which are mainly determined by the boundary condition of almost zero electric field along the centres of the non-saturated filaments. The current paths are closed across the normal conducting matrix in which the heat is generated.

The interfilament coupling loss (IFCL) can be calculated using an anisotropic continuum model [Carr, '74] based on solving Maxwell's equations. Here another approach, proposed by Morgan, is followed based on the calculation of the induced currents between two twisted filaments in a strand [Morgan, '70]. The strand is assumed to have a circular cross-section with diameter d_s in which the filaments are arranged in concentric layers. Two filaments of the outer concentric layer, with diameter d_s^*, are shown in Fig. 3.5.

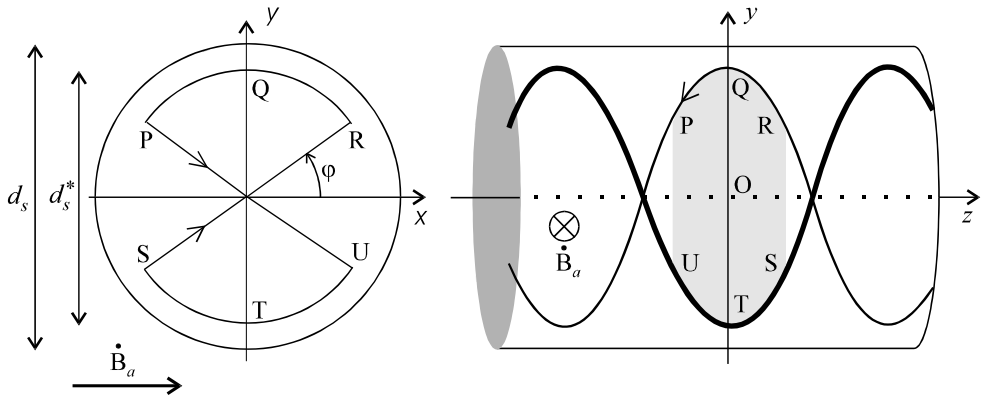

Figure 3.5. Cross-section of a strand and schematic view of a current path RQPUTS in which an electromotive force is generated due to an external applied-field variation.

If the strand is subjected to a varying magnetic field $\dot{\mathbf{B}}_a$ in the *x*-direction, a field change $\dot{\mathbf{B}}_i$ is induced by the interfilament coupling currents (IFCCs), so that the total field change $\dot{\mathbf{B}}_s$ in the interior equals:

$$\dot{\mathbf{B}}_s = \dot{\mathbf{B}}_a + \dot{\mathbf{B}}_i \quad [\mathrm{Ts}^{-1}] \,. \tag{3.9}$$

The homogeneous $\dot{\mathbf{B}}_a$ over the whole cross-section will result in a homogeneous $\dot{\mathbf{B}}_i$, parallel to $\dot{\mathbf{B}}_a$, and thus in a homogeneous $\dot{\mathbf{B}}_s$. The induced voltage $U_{ind}(z)$ is obtained from the surface RQPUTS:

$$U_{ind}(z) = -\int \dot{B}_s dA = -4\frac{1}{2} d_s^* \dot{B}_s \int_0^z \cos(2\pi z / L_{p,f})\, dz = -2 d_s^* \left(\frac{L_{p,f}}{2\pi} \right) \dot{B}_s \cos(\varphi) \quad [\mathrm{V}], \tag{3.10}$$

with $L_{p,f}$ the twist pitch of the filaments and $\varphi = (\pi/2 - 2\pi z / L_{p,f})$.

Since there is no voltage drop along the superconducting filament, the voltage of any filament with position φ in a cross-section relative to the *z*-axis is:

$$U(\varphi) = -\frac{1}{4}U_{ind}(z) = \left(\frac{L_{p,f}}{2\pi}\right)\frac{d_s^* \dot{B}_s}{2}\cos(\varphi) \quad [\mathrm{V}] . \tag{3.11}$$

Since $x = d_s^* \cos(\varphi)/2$ the voltage will give rise to a homogeneous electric field parallel to $\dot{\mathbf{B}}_a$:

$$\mathbf{E}_{\|} = -\frac{L_{p,f}}{2\pi}\dot{\mathbf{B}}_s \quad [\mathrm{Vm^{-1}}] . \tag{3.12}$$

The *z*-component of the electric field, which is present due to the twist angle, is not taken into account. Since $\mathbf{E}_{\|}$ is independent of d_s^* the solution holds for all filaments and therefore also for the complete strand. The electric field $\mathbf{E}_{\|}$ creates a current density $\mathbf{J}_{\|}$ flowing across the strand parallel to $\dot{\mathbf{B}}_s$:

$$\mathbf{J}_{\|} = -\left(\frac{L_{p,f}}{2\pi}\right)\frac{\dot{\mathbf{B}}_s}{\rho_{eff}} \quad [\mathrm{Am^{-2}}] , \tag{3.13}$$

with ρ_{eff} the effective transverse resistivity which depends on the filling factor η as [Carr, '75]:

$$\rho_{eff}(\eta) = \rho_{mat}\left(\frac{1-\eta}{1+\eta}\right) \text{ or } \rho_{eff}(\eta) = \rho_{mat}\left(\frac{1+\eta}{1-\eta}\right) \quad [\Omega\mathrm{m}] , \tag{3.14}$$

whenever the filaments do or do not contribute to the transverse conduction respectively. The resistivity ρ_{mat} denotes the transverse resistivity of the matrix.

The current density $\mathbf{J}_{\|}$ gives rise to a coupling power loss per unit volume:

$$P_{if} = J_{\|}E_{\|} = \left(\frac{L_{p,f}}{2\pi}\right)^2 \frac{\dot{B}_s^{\,2}}{\rho_{eff}} \quad [\mathrm{Wm^{-3}}] . \tag{3.15}$$

The outer layer of filaments act as a return path for $\mathbf{J}_{\|}$ so that the collected current I_f in the filaments (using the continuity of current) satisfies:

$$\frac{dI_f(\varphi)}{dz} = J_{\|}\cos(\varphi) \quad [\mathrm{Am^{-2}}] . \tag{3.16}$$

Integration results in the induced axial surface current density $I_f(\varphi)$ in the *z*-direction:

$$I_f(\varphi) = -\left(\frac{L_{p,f}}{2\pi}\right)^2 \frac{\dot{B}_s}{\rho_{eff}}\sin(\varphi) \quad [\mathrm{Am^{-1}}] . \tag{3.17}$$

Assuming that the current flows through the outer layer of filaments at radius $d_s^*/2$, the total current I_{if} flowing at either side of the strand (positive at one side and negative at the other side) equals:

$$I_{if} = \pm 2 \int_0^{\pi/2} I_f(\varphi) d_s^* d\varphi = \pm \left(\frac{L_{p,f}}{2\pi} \right)^2 \frac{d_s^* \dot{B}_s}{\rho_{eff}} \quad [\mathrm{A}] . \tag{3.18}$$

Since $I_f(\varphi)$ varies with $\sin(\varphi)$, a uniform dipole-field $\mathbf{B}_i$ in the interior of the strand is generated parallel and opposite to $\dot{\mathbf{B}}_a$:

$$\mathbf{B}_i = \frac{\mu_0}{2d_s^*} I_{if} = -\left(\frac{L_{p,f}}{2\pi} \right)^2 \frac{\mu_0 \dot{\mathbf{B}}_s}{2\rho_{eff}} = -\tau_{if} \dot{\mathbf{B}}_s \quad [\mathrm{T}] . \tag{3.19}$$

The constant of proportionality τ_{if} is called the time constant of the IFCCs, and defined by:

$$\tau_{if} = \frac{\mu_0}{2\rho_{eff}} \left(\frac{L_{p,f}}{2\pi} \right)^2 \quad [\mathrm{s}] . \tag{3.20}$$

The time constant increases by a factor of about 1.27 for square strands [Campbell, '82] and by a factor $[1+(\pi d_s/L_{p,f})^2]$ if the *z*-component of the electrical field is also taken into account (which is about 1.02 for a characteristic ratio $d_s/L_{p,f}=0.05$).

Combining eqs. 3.9 and 3.19 gives the relation between the applied field and the internal field by means of the differential equation:

$$\dot{\mathbf{B}}_i + \frac{\mathbf{B}_i}{\tau_{if}} = -\dot{\mathbf{B}}_a \quad [\mathrm{Ts^{-1}}] . \tag{3.21}$$

The energy loss Q_{if} per cycle and per unit volume is determined by integration of eq. 3.15. For a sinusoidally oscillating applied field:

$$B_a = B_a^m \cos(\omega t) \quad [\mathrm{T}] , \tag{3.22}$$

with amplitude B_a^m and angular frequency $\omega = 2\pi f$, the energy loss equals:

$$Q_{if} = \oint P_{if}\, dt = \frac{2\tau_{if}\, \pi\omega (B_a^m)^2}{\mu_0 \left(1+(\omega\tau_{if})^2 \right)} \quad [\mathrm{Jm^{-3}/cycle}] . \tag{3.23}$$

Using the anisotropic continuum model, a basically identical relation is obtained [Carr, '74].

More generally, the factor 2 in eq. 3.23 should be replaced by the shape factor *n*, which is equal to 2 for round and square wires. In the case of rectangular strands with a cross-section $a \cdot b$ where $a \gg b$, $n = 1$ for $\dot{\mathbf{B}}_a$ applied perpendicular to *b* and $n = a/b$ for $\dot{\mathbf{B}}_a$ applied perpendicular to *a* [Campbell, '82].

At low field amplitudes the magnetic moment of the filaments is large and the filaments can even become perfectly diamagnetic. In this case the strand should be treated as a material with an effective permeability [Campbell, '82]:

$$\mu_{eff} = \frac{n(1-\lambda)}{2\lambda + n(1-\lambda)} = (1-\lambda) \text{ for } n = 2 \quad [\text{Hm}^{-1}] , \tag{3.24}$$

with λ the copper-to-superconductor ratio. This results in a decrease of the time constant to $\tau_{if,eff} = \mu_{eff}\, \tau_{if}$ (where τ_{if} is the time constant when the filaments are completely penetrated), and in a decrease of the coupling power loss by a factor μ_{eff}. So the energy loss equals:

$$Q_{if} = \frac{n \tau_{if} \pi \mu_{eff}^2 \omega (B_a^m)^2}{\mu_0 \left(1 + (\mu_{eff} \omega \tau_{if})^2\right)} \quad [\text{Jm}^{-3} \text{ per cycle}] , \tag{3.25}$$

and is significantly smaller compared to eq. 3.23 at low frequencies ($\omega \tau_{if} \ll 1$).

The above-mentioned relations are valid as long as the currents in the filaments in the outer layer do not exceed the critical current. Beyond this limit the filaments become saturated and the excess currents have to return via the filaments in the more inner layers, which causes a decrease in the induced magnetic field B_i. The losses in a multifilamentary strand can therefore be classified in three frequency ranges:

- Low frequency, $\omega \tau_{if} \ll 1$. The inside of the strand is subjected to the external field since the screening by the IFCCs is very small. The hysteresis loss can be treated independently of the IFCL.
- Intermediate frequency, $\omega \tau_{if} \geq 1$. The inside of the strand is partially shielded by the IFCCs but the fields are still uniform. Due to the screening, the hysteresis loss is smaller than in the low-frequency range.
- High frequency, $\omega \tau_{if} \gg 1$. The inside of the strand is almost completely shielded since the applied field penetrates only a thin skin of the strand. The hysteresis loss approaches zero because only the outer layers of filaments are subjected to a field change.

As τ_{if} is typically of the order of 10-100 ms, especially the first frequency range will be of interest in the case of the slowly varying fields which are present in accelerator magnets. Therefore, the decrease of the hysteresis due to the screening of the IFCCs is not discussed here, but an extensive treatment can be found in the literature [Pang, '80].

The characteristic distribution of the IFCCs over the cross-section of the strand is depicted in Fig. 3.6. Three different regions (besides the normal conducting core and outer shell) can be distinguished:

– region I: the filaments are completely saturated,
– region II: the filaments are partially saturated,
– region III: the filaments do not carry any IFCCs.

As a result, the transport current can only flow in region III, since a transport current flowing in region II would also pass through region I (due to the twist), thereby generating an additional loss.

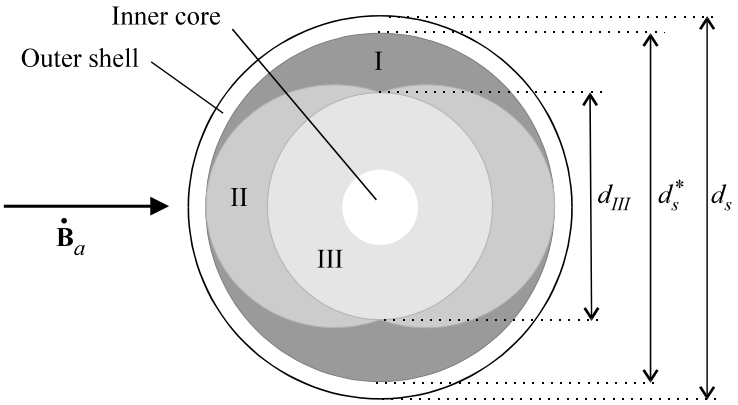

Figure 3.6: Current distribution in a wire without transport current, subject to a varying magnetic field, indicating three different regions: **I.** the filaments are completely saturated by the IFCCs, **II.** the filaments are partially saturated by the IFCCs, **III.** the filaments carry no IFCCs. The current profile is calculated by disregarding the influence of the central core.

The calculated diameter d_{III} of region III, where the filaments do not carry IFCCs and after disregarding the inner core [Klundert, van de, '90], equals:

$$d_{III} = d_s^* \left(1 - \frac{L_{p,f}\,\dot{B}_a}{2\pi\eta J_C\,\rho_{eff}} \right) = d_s^* \left(1 - \frac{4\pi\tau_{if}\,\dot{B}_a}{\eta J_C\,\mu_0 L_{p,f}} \right) \quad \text{[m] for } \dot{B}_a L_{p,f} < 2\pi\eta J_C\,\rho_{eff}\,. \quad (3.26)$$

Hence, the maximum transport current $I_{tr,str,max}$ in a strand is not only a function of the temperature and the applied magnetic field but also of the rate of change of the magnetic field. As the boundaries of the three regions are not influenced by a transport current [Hartmann, '89], $I_{tr,str,max}$ can be expressed by:

$$I_{tr,str,max}(B_a, \dot{B}_a, T) = I_{C,str}(B_a, T)(d_{III} / d_s^*)^2 \quad \text{[A]}\,, \quad (3.27)$$

which corresponds to within 5% with a more complicated relation given by Hartmann. Experimental results are in agreement with the above-mentioned expression [Rem, '85], [Roovers, '86]. Eq. 3.27 can be rewritten in terms of τ_{if} using eqs. 3.20 and 3.26:

$$I_{tr,str,max}(B_a, \dot{B}_a, T) = I_{C,str}(B_a, T) \left(1 - \frac{(\pi d_s^*)^2\,\tau_{if}\,\dot{B}_a}{I_{C,str}(B_a, T)\,\mu_0 L_{p,f}} \right)^2 \quad \text{[A]}\,. \quad (3.28)$$

In sections 3.5 and 8.2.1 the relation is applied to estimate the decrease of the maximum transport current due to the IFCCs.

Practical conductors are often subdivided into several regions. A very common lay-out consists of the following three concentric layers with volume fractians v_1, v_2 and v_3 respectively (see Figs. 2.9a and 3.6):

– a central core of normal-conducting material with resistivity ρ_1,
– a ring filled with many filaments in a matrix with resistivity $\rho_2 = \rho_{eff}$,
– an outer shell of normal-conducting material with resistivity ρ_3.

Characteristic values for v_1, v_2 and v_3 for NbTi strands for accelerator magnets are 0.15, 0.75 and 0.10 respectively. The loss contributions of each layer for $\omega \tau_{if} < 1$ can be summarised by [Kate, ten, '94]:

$$P_{if,1} = v_1 \left(\frac{L_{p,f}}{2\pi} \right)^2 \frac{\dot{B}_s^2}{\rho_1} \quad [\mathrm{Wm}^{-3}] , \tag{3.29}$$

$$P_{if,2} = v_2 \left(\frac{L_{p,f}}{2\pi} \right)^2 \frac{\dot{B}_s^2}{\rho_{eff}} \quad [\mathrm{Wm}^{-3}] , \tag{3.30}$$

$$P_{if,3} = v_3 \frac{v_1 + v_2}{v_1 + v_2 + 1} \left(\frac{L_{p,f}}{2\pi} \right)^2 \frac{\dot{B}_s^2}{\rho_3} \quad [\mathrm{Wm}^{-3}] . \tag{3.31}$$

For $\rho_1 = \rho_2 = \rho_{eff}$, the subdivision in regions decreases the IFCL of the LHC strands by a factor of about 0.9 compared to eq. 3.15. If the filaments contribute to the transverse resistivity (see eq. 3.14), the decrease is a factor of about 0.8 for $\eta = 0.35$.

3.5 Interfilament time constants

The measurement set-up as described in section 3.3 is used to evaluate the IFCL of a cable, determined by the increase of the area of the *M-B* curve for higher frequencies. The field is applied parallel to the cable width ($\theta = \varphi = 90°$, see Fig. 4.1). This implies that the magnetisation is mainly determined by the hysteresis of the filaments and the interfilament coupling while the interstrand coupling is negligible, even for relatively low interstrand contact resistances (see section 4.4.1). Magnetisation loops of cable I-2 are shown in Fig. 3.7 for several frequencies.

At higher frequencies $f = \omega / 2\pi$ the curves become more and more elliptical with a phase shift between the internal field and the external field (according to eq. 3.21), equal to $\arctan(\omega \tau_{if})$.

A more accurate method to determine the time constant τ_{if} is by calculating the total energy loss per cycle:

$$Q_{tot} = Q_{hys} + Q_{if} \quad [\mathrm{J/cycle}] , \tag{3.32}$$

by the surface of the *M-B* curve, as a function of the frequency (see Fig. 3.8). The time constant can be deduced from the maximum of the Q_{tot}-f relation. Note that the hysteresis loss decreases at higher frequencies due to the screening of the IFCCs which results in a shift of the maximum of the curve to slightly lower frequencies. The apparent increase of τ_{if} could be significant when the IFCL is small compared to the hysteresis loss.

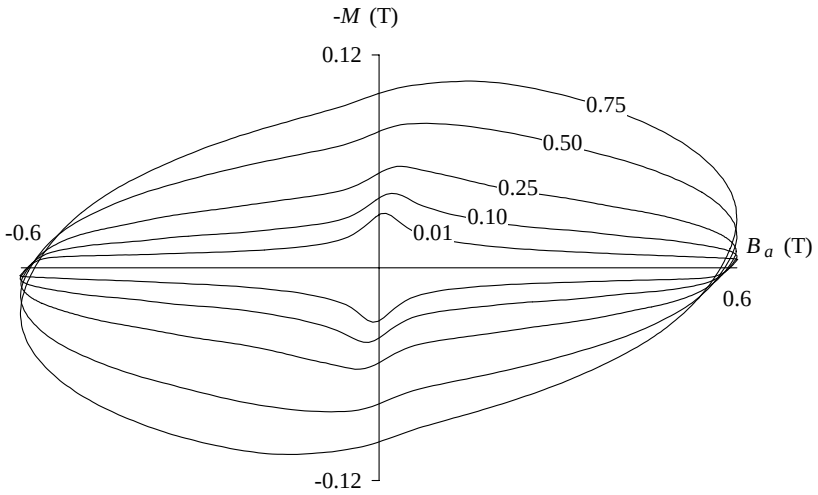

Figure 3.7. Magnetisation loops of cable I-2 exposed to an oscillating applied field with amplitude $B_a^m = 0.6$ T at frequencies of 0.01, 0.1, 0.25, 0.5 and 0.75 Hz (without transport current).

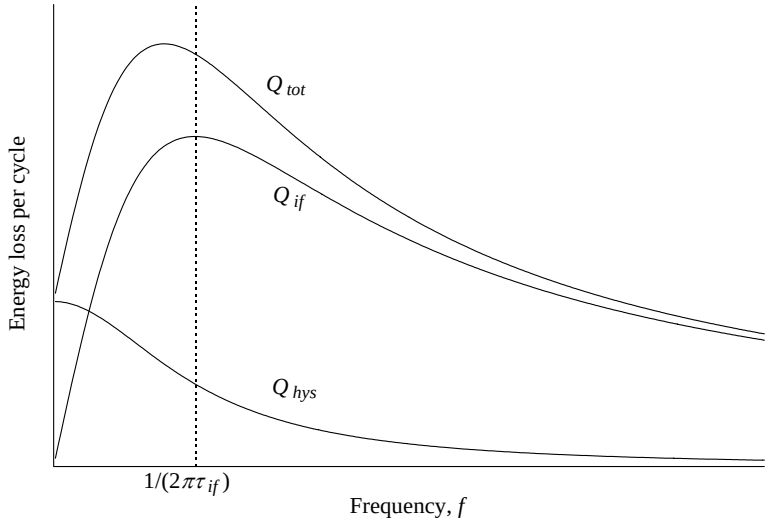

Figure 3.8. Characteristic Q_{tot}-f relation for conductors which exhibit hysteresis loss and IFCL. A frequency-dependent hysteresis loss is assumed [Pang, '80]. Note that the apparent time constant calculated from the maximum of the Q_{tot}-f curve, increases due to the screening of the interior of the strand by the IFCCs.

Here $n\tau_{if}$ is determined from the slope of the Q_{tot}-f relation for $f \to 0$ according to eq. 3.25 assuming μ_{eff}=1. The Q_{tot}-f relation of various samples exposed to a field sweep from -0.6 to 0.6 T is shown in Fig. 3.9. Table 3.2 shows a survey of the τ_{if}-values of the samples assuming n=2.

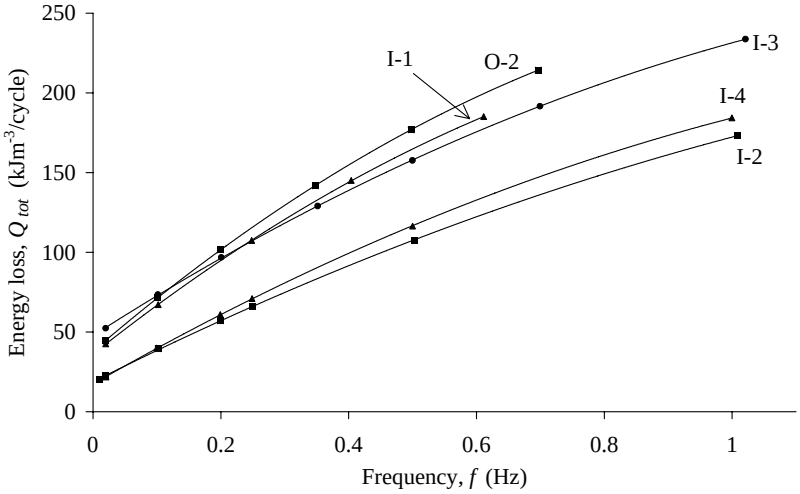

Figure 3.9. The total energy loss of various cables as specified in Table 2.4 exposed to a field sweep between -0.6 and 0.6 T at frequencies between 0.02 and 1 Hz.

The ratio d_{III}/d_s^* as calculated using eq. 3.26 for $n=2$, $\dot{B}_a=0.1$ Ts^{-1} and $I_C=500$ A is also given. The corresponding decrease of the maximum transport current (according to eq. 3.27) is smaller than 1% at $\dot{B}_a=0.1$ Ts^{-1} and smaller than 0.05% at $\dot{B}_a=0.0066$ Ts^{-1}, the average field-sweep rate during excitation as foreseen for the LHC dipole magnets, and will therefore not affect the maximum operation field in the magnets. In practice the decrease is even smaller since $I_{C,str}$ increases if the transport current decreases (see also section 8.2) and because the time constant decreases at higher fields due to the magnetoresistance of the matrix.

Table 3.2. Survey of the τ_{if}-values of several cables as deduced from the slope of Q_{tot}-f relation with $B_a{}^m=0.60$ T and assuming $n=2$. The calculated relative decrease i of the maximum transport current is included for a field-sweep rate of 0.1 Ts^{-1} (with $I_{C,str}=500$ A).

	I-1	I-2	I-3	I-4	O-2
τ_{if} (ms)	29	23	26	24	32
d_{III}/d_s^* at 0.1 Ts^{-1} (mm)	0.997	0.998	0.997	0.998	0.999
i at 0.1 Ts^{-1}	0.994	0.995	0.995	0.995	0.997

In order to investigate the influence of adjacent strands on the hysteresis loss and IFCL, individual strands are removed from cable I-4 and kept in the original shape they have in the cable. The sample is referred to as I-4o.

Fig. 3.10 shows the ratio of the energy loss per cycle per volume between I-4 and I-4o as a function of the frequency. In the case of a large B_a^m (compared to the penetration field) and low frequencies, the field produced by the neighbouring strands is small compared to the applied field and the ratio approaches 1.

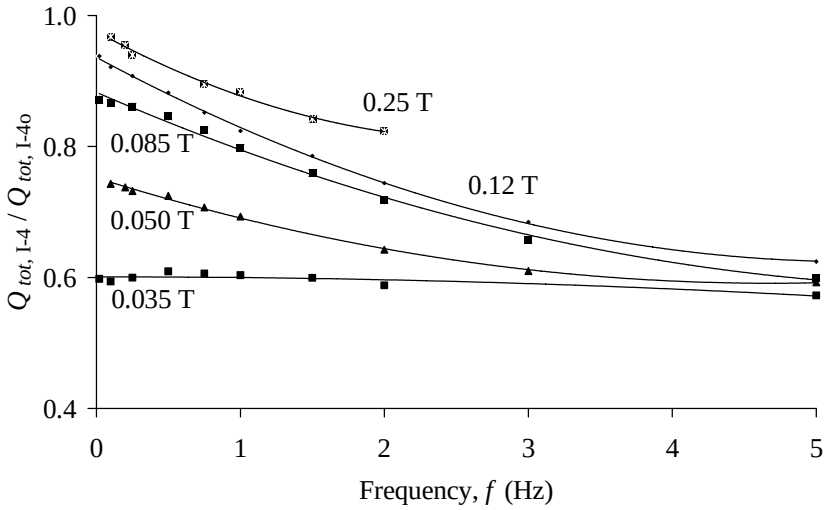

Figure 3.10. The energy loss (per unit volume) of the cable I-4 divided by the energy loss (per unit volume) of a strand in the 'cable shape' I-4o as a function of the frequency for several amplitudes of the applied field.

For small B_a^m the field produced by the persistent currents of the neighbouring strands is not negligible compared to the applied field and the demagnetisation of the cable becomes relevant, resulting in a ratio smaller than 1. Considering larger frequencies, the additional field produced by the IFCCs (being opposite to the applied field), reduces the total field, especially in the centre of the cable. This implies an even stronger decrease of the loss in the cable compared to the loss in individual strands.

The field variations in accelerator magnets are large and quasi DC; for example, the characteristic ramp for the LHC dipole magnets corresponds to a field sweep of about 8 T in 20 minutes. Even the fast de-excitation with a time constant of 100 s can be classified in the $\omega\tau_{if}<1$ regime. Hence, the hysteresis loss and IFCL in accelerator magnets can be directly determined by the losses in a single strand, and are not affected by the field produced by the persistent currents and IFCCs in the neighbouring turns.

3.6 Conclusions

Filament hysteresis and interfilament coupling are the main sources of loss inside a strand which is exposed to a varying magnetic field. The two loss components can be well separated by determining the magnetisation vs. frequency in the range $\omega\tau_{if}<1$. In the case of larger frequencies the interior of the strand becomes partially or almost completely shielded by the screening currents and the hysteresis is no longer independent of the frequency. An additional transport current increases the hysteresis loss by a factor $(1+(J_{tr}/J_C)^2)$.

The strand losses (per unit volume) in an LHC-type NbTi cable are identical to the losses in a single strand (per unit volume), under the same conditions, if the applied field amplitude is large (compared to the penetration field) and the frequency is small ($<1/(2\pi\tau_{if})$). In the case of small field amplitudes and/or high frequencies the demagnetisation of the cable will cause a considerable decrease of the losses. The strand losses in dipole magnets, subject to a central-field sweep, which is large compared to the penetration field, can therefore be succesfully estimated by a loss measurement on a single strand.

The mean time constants τ_{if} of the interfilament coupling currents for various cables used in the LHC dipole model magnets are between 23 and 33 ms. The corresponding decrease in the maximum transport current due to the the IFCCs during the field sweep from injection to operating field in LHC magnets will be smaller than 0.05% (not taking into account the possible temperature increase of the cable due to the loss).